JACS
JOURNAL OF THE AMERICAN CHEMICAL SOCIETY
Article
pubs.acs.org/JACS

Syntheses of Water-Soluble Octahedral, Truncated Octahedral, and Cubic Pt–Ni Nanocrystals and Their Structure–Activity Study in Model Hydrogenation Reactions

Yuen Wu,[†] Shuangfei Cai,[†] Dingsheng Wang,[†] Wei He,[‡,§,*] and Yadong Li[†,*]

[†]Department of Chemistry, Tsinghua University, Beijing, 100084 People's Republic of China
[‡]Tsinghua-Peking Center for Life Sciences, Tsinghua University, Beijing, 100084 People's Republic of China
[§]School of Medicine, Tsinghua University, Beijing 100084 People's Republic of China

Supporting Information

ABSTRACT: We developed a facile strategy to synthesize a series of water-soluble Pt, Pt_xNi_{1-x} ($0 < x < 1$), and Ni nanocrystals. The octahedral, truncated octahedral, and cubic shapes were uniformly controlled by varying crystal growth inhibition agents such as benzoic acid, aniline, and carbon monoxide. The compositions of the Pt_xNi_{1-x} nanocrystals were effectively controlled by choice of ratios between the Pt and Ni precursors. In a preliminary study to probe their structure–activity dependence, we found that the shapes, compositions, and capping agents strongly influence the catalyst performances in three model heterogeneous hydrogenation reactions.

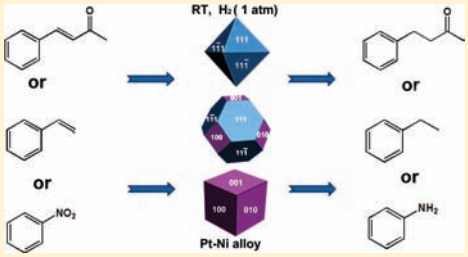

INTRODUCTION

Noble metal nanoparticles (NPs) (i.e., Pt,[1] Pd,[2,3] etc.) with well-defined sizes, compositions, and facets have been widely used as catalysts in many applications such as organic reactions,[4] fuel cells,[5] and so on.[6] To improve atomic efficiency and sustainability, researchers have studied the Pt-based bimetallic nanostructures in which Pt is partially replaced by cheap 3d-transition metals (i.e., Fe, Co, Ni, etc.) as promising substitutions.[7,8] Importantly, previous research showed that bimetallic nanostructures could exhibit superior catalytic performances, possibly due to the different geometric and electronic structures brought by the introduction of the second metal.[9,10]

The hydrogenation reactions of benzalacetone, styrene, and nitrobenzene are important industrial processes[11−13] in which homogeneous catalysts have been widely used, but the recycling of catalysts remains difficult. Owning high selectivity for the desired product without sacrificing activity, heterogeneous catalysts[14] have attracted much attention for the ease of their separation and recycling.[15,16] Among them, bimetallic catalysts are intriguing for possible synergistic effects that allow hydrogenation reactions under relatively mild conditions.

In this work, we developed a general method for the shape controlled synthesis of a series of water-soluble Pt, Pt_xNi_{1-x} ($0 < x < 1$) and Ni nanocrystals, which utilizes a capping agent poly (vinylpyrrolidone) (PVP) that exempted the catalyst from postsynthesis treatment. As a complement to the hydrophilic system, the water-soluble catalysts produced by this method are also compatible with hydrophobic solvents through a ligands exchange process. The shapes of octahedral, truncated octahedral, and cubic Pt–Ni alloy were controlled by varying the growth inhibition agent such as benzoic acid, aniline, carbon monoxide, and potassium bromide. In a preliminary structure–activity study, we found that the rate of hydrogenation of benzalacetone, styrene, and nitrobenzene were significantly affected by the shape, composition, and surface of as-prepared nanocrystals. We found that the octahedral $PtNi_2$ alloy exhibited superior reactivity than Pt–Ni truncated octahedrons and cubes. Furthermore, the Pt–Ni alloy octahedral nanocrystal was much more effective than its monometallic counterparts, effecting the hydrogenation of the C=C and N=O bonds in high yield at room temperature under atmosphere pressure with great selectivity.

EXPERIMENTAL SECTION

Chemicals. Analytical grade benzyl alcohol, aniline benzaldehyde, benzoic acid, and salicylic acid were obtained from Beijing Chemical Reagents, P.R. China. Pt(acac)2 (99%), Ni(acac)2 (99%), and PVP (MW = 8000, AR) were purchased from Alfa Aesar. All of the chemicals were used without further purification.

Characterization. The crystalline structure and phase purity were determined using a Rigaku RU-200b X-ray powder diffractometer with CuKa radiation (l = 1.5418 Å) and a FEI Tecnai G2 F20 S-Twin high-resolution transmission electron microscopy (HRTEM). The composition of the product was measured by the inductively coupled plasma atomic emission spectroscopy (ICP-AES) and energy dispersive spectrometer (EDS). The catalysts' sizes and morphologies were analyzed on a Hitachi H-800 transmission electron microscope (TEM) and a FEI Tecnai G2 F20 S-Twin high-resolution transmission electron microscope (HRTEM). X-ray photoelectron spectroscopy (XPS) experiments were performed on a ULVAC PHI Quantera microprobe. Binding energies (BE) were calibrated by setting the measured BE of C 1s to 284.8 ev. The catalytic reaction result was

Received: March 17, 2012
Published: April 22, 2012

   dx.doi.org/10.1021/ja302606d | J. Am. Chem. Soc. 2012, 134, 8975–8981

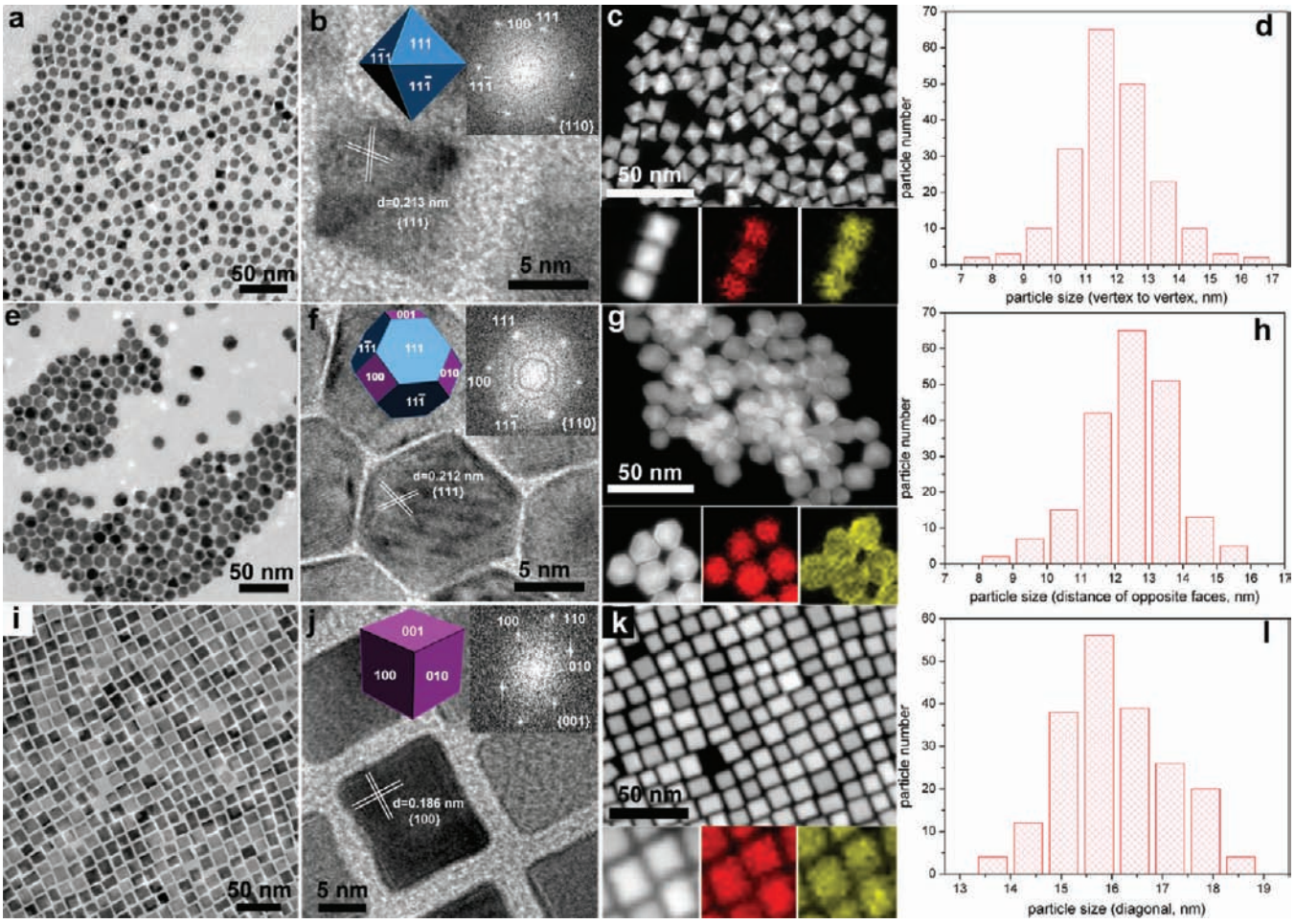

Figure 1. (a) TEM, (b) HRTEM (Top-right and top-middle insets show the corresponding FFT pattern and the ideal structure model), and (c) HAADF-STEM images of $PtNi_2$ octahedrons, corresponding element maps showing the distribution of Pt (yellow) and Ni (red). (d) Size distribution of octahedral particles (average size: 11.8 ± 1.2 nm, 95% octahedrons and 5% irregular shapes). (e) TEM, (f) HRTEM, and (g) HAADF-STEM images of $PtNi_2$ truncated octahedrons. (h) Size distribution of truncated octahedral particles (average size: 12.5 ± 1.1 nm, 90% truncated octahedrons and 10% irregular shapes). (i) TEM, (j) HRTEM, and (k) HAADF-STEM images of $PtNi_2$ cubes. l) Size distribution of cubic particles (average size: 16.1 ± 1.7 nm, 95% octahedrons and 5% irregular shapes).

measured by gas chromatography (GC) (SP-6890) and gas chromatography–mass spectroscopy (GC–MS) (ITQ 700/900/1100) and ^{1}H NMR. The NMR spectroscopy was conducted on a JEOL JNM-ECX 400 MHz instrument.

Preparation of Pt and Pt_xNi_{1-x} ($0 < x < 1$) Octahedral and Truncated Octahedral Nanocrystals. In a typical synthesis of Pt and Pt_xNi_{1-x} ($0 < x < 1$) octahedral nanocrystals, $Pt(acac)_2$, (8.0 mg), poly(vinylpyrrolidone) (PVP, MW = 8000, (80.0 mg) $Ni(acac)_2$ (ranging from 0 mg to 500 mg) and benzoic acid (50 mg) were dissolved in 5 mL of benzylalcohol, followed by 10 min vigorous stirring. The resulting homogeneous green solution was transferred into a 12-mL Teflon-lined stainless-steel autoclave. The sealed vessel was then heated at 150 °C for a 12 h before it was cooled down to room temperature. The products were precipitated by acetone, separated via centrifugation, and further purified by an ethanol–acetone mixture. The truncated octahedral nanocrystals were synthesized followed the above procedure by replacing the benzoic acid (50 mg) with aniline (0.1 mL).

Preparation of Pt and Pt_xNi_{1-x} ($0 < x < 1$) Cubic Nanocrystals. In a typical synthesis of Pt and Pt_xNi_{1-x} ($0 < x < 1$) cubic nanocrystals, $Pt(acac)_2$, (8.0 mg), poly(vinylpyrrolidone) (PVP, MW = 8000, (80.0 mg)), $Ni(acac)_2$ (ranging from 0 mg to 150 mg) and potassium bromide (50.0 mg) were dissolved in 5 mL of benzylalcohol, followed by 10 min vigorous stirring. The resulting homogeneous green solution was transferred into a 10-mL round-bottom flask equipped with a magnetic stirrer. The reaction flask was immersed in an oil bath at 25 °C. After being pumped on a vacuum line for 30 min, the flask was then transferred to a second oil bath at 150 °C under a carbon monoxide balloon. After another 4 h, the black nanoparticles were precipitated by acetone, separated via centrifugation, and further purified by an ethanol–acetone mixture.

Preparation of Ni Octahedral and Truncated Octahedral Nanocrystals. In a typical synthesis of octahedral Ni nanocrystals, poly(vinylpyrrolidone) (PVP, MW = 8000, (80.0 mg)), $Ni(acac)_2$ (10 mg), benzaldehyde (0.5 mL) and benzoic acid (50.0 mg) were mixed together with benzylalcohol (5 mL). The resulting homogeneous green solution was transferred into a 12-mL Teflon-lined stainless-steel autoclave. The sealed vessel was then heated at 200 °C for 12 h before it was cooled to room temperature. The black nanoparticles were precipitated by acetone, separated via centrifugation, and further purified by an ethanol–acetone mixture. The Ni truncated octahedron was synthesized using the above procedure with aniline (0.1 mL) instead of benzaldehyde and benzoic acid.

Typical Procedure for the Hydrogenation of Benzalacetone, Styrene, and Nitrobenzene Catalyzed by Octahedral $PtNi_2$. To a 25 mL round flask was charged a solution of the respective substrate (0.5 mmol benzalacetone, or styrene, or nitrobenzene) in THF (2.5 mL) and the octahedral $PtNi_2$ (0.01 mmol, 2 mol %). After being purged with H_2, the reaction mixture was stirred at room temperature under a H_2 balloon. When GC monitoring indicates the complete consumption of the substrate, (see GC detailed conditions in Table S1 of the Supporting Information, SI) the octahedral $PtNi_2$ was separated

dx.doi.org/10.1021/ja302606d | J. Am. Chem. Soc. 2012, 134, 8975–8981

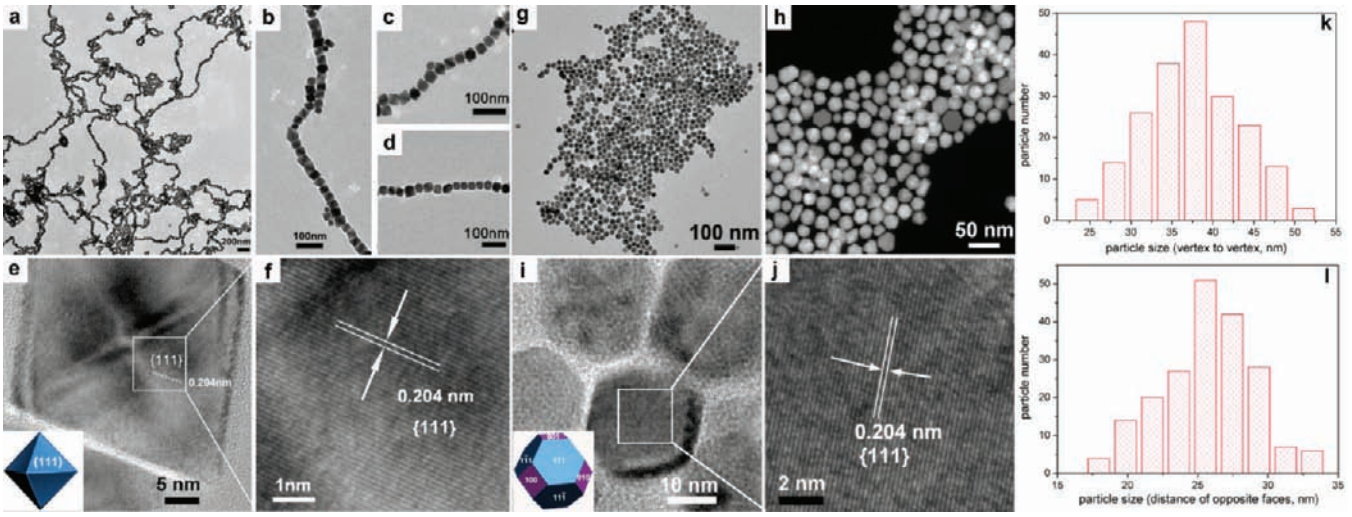

Figure 2. (a)TEM image of Ni octahedrons (b–d) Magnified TEM images of Ni 1D structures with different orientation (e) HRTEM image of Ni octahedron; the inset is the scheme of the structure of octahedron; (f) Magnified images of the lattice fringe of the Ni octahedron. (g) TEM, (h) HAADF-STEM, and (i) images of Ni truncated octahedrons. (j) Magnified images of the lattice fringe of the Ni truncated octahedron Size distributiong of (k) octahedral Ni nanoparticles (average size: 40.0 ± 5.1 nm, 90% octahedrons, and 5% irregular shapes) and (l) truncated octahedral Ni nanoparticles (average size: 25.2 ± 4.3 nm, 80% octahedrons, 15% nanoplate, and 5% irregular shapes).

from the mixture by a magnet and the liquid phase was concentrated under reduced pressure. The product was purified by column chromatography and subsequently characterized by ^{1}H NMR.

Preparation of Oleylamine-Capped $PtNi_2$ Nanocrystals. In a typical synthesis of oleylamine-capped $PtNi_2$ nanocrystals, $PtNi_2$ NPs (10.0 mg) were dispersed in chloroform (5 mL) in a 25 mL vial and to this vial oeylamine (0.1 mL) was added. The resulting mixture was sonicated for 5 min before it was refluxed for 1 h. The oleylamine-capped $PtNi_2$ nanocrystals were obtained by centrifugation at 10 000 rpm for 10 min and subsequently purified by the ethanol–cyclohexane mixture.

Preparation of Clean $PtNi_2$/C (10% Loading) from Oleylamine-Capped $PtNi_2$ Nanocrystals. In a typical synthesis of clean $PtNi_2$/C, oleylamine-capped $PtNi_2$ NPs (10 mg) were dispersed in 5 mL of cyclohexane in a 25 mL vial and to this vial active carbon (100.0 mg) was added. This colloidal mixture was sonicated for 2 h. The solid was first obtained by centrifugation at 10 000 rpm for 10 min and then washed by the ethanol–cyclohexane (5 to 5 mL) mixture. The as-prepared solid was dispersed in 20 mL of acetic acid and heated at 70 °C for 10 h. The clean $PtNi_2$/C was finally obtained by centrifugation at 10 000 rpm for 10 min, washed by ethanol and water for 3 times and dried in an oven (60 °C).

Catalyst Recovery. The $PtNi_x$ ($x \geq 1$) and Ni colloid catalysts were separated from the reaction mixture by a magnet. After being washed with ethanol (3 times), the recovered catalysts were directly used in the next cycle of the reaction without further manipulations.

RESULTS AND DISCUSSION

Octahedral Pt_xNi_{1-x}($0 < x < 1$) Nanocrystals. The representative transmission electron microscopy (TEM) images (Figure 1) showed that the as-prepared $PtNi_2$ nanocrystals were all uniform in terms of the narrow size distribution and exclusively bound by well-defined {111} or {100} facets. The high resolution TEM (HRTEM) images and fast Fourier transform (FFT) images (Figure 1b,f,j) on single NP both confirmed their single-crystalline nature. Continuous lattice fringes measurements with an interplanar spacing of 0.213 and 0.186 nm could be assigned to the corresponding {111} facets and {100} facets of fcc Pt–Ni alloy, respectively.

The octahedral particles have an average distance of 11.8 ± 1.2 nm from one apex to the opposite apex and consist of only eight equivalent {111} facets. The high-angle annular dark-field scanning transmission electron microscope (HAADF-STEM) micrographs showed that all the surfaces of the octahedrons were smooth without obvious defect throughout the nanocrystal. The corresponding elemental maps of HAADF-STEM (Figure 1c) showed that both Pt and Ni were distributed evenly throughout each individual $PtNi_2$ alloy octahedral nanocrystal. To realize the formation of Pt–Ni octahedrons, we envisioned a reaction that involved benzoic acid produced by the oxidation process of benzoic alcohol. Indeed, the yields of octahedrons significantly increased from 40% to 70%, and 95% with the amounts of benzoic acid from 0 mol to 0.04 mmol, and 0.4 mmol. In contrast, the yield was almost unaffected by increasing the amount of benzoic acid from 0.4 to 2.0 mmol. Herein, the usage of benzoic acid was believed to promote the formation of octahedral NPs, while the absence of benzoic acid resulted in the formation of Pt–Ni with mixed morphologies (Figure S3 of the SI).

Truncated Octahedral Pt_xNi_{1-x}($0 < x < 1$) Nanocrystals. By replacing benzoic acid with aniline, we could obtain a series of Pt–Ni alloy with truncated octahedral shape. The truncated octahedrons consisted of both {100} and {111} facets and the average distance of two opposite faces was 12.5 ± 1.1 nm (Figure 1e). In our synthetic method, the benzoic alcohol was used as solvent and reductant, however the addition of aniline was believed to add as reductant and affect the reaction kinetics. The sizes of truncated octahedral $PtNi_2$ NPs could be tuned from 16.0 to 12.5 nm, 7.2 nm, and 4.8 nm by varying the quantity of aniline. Some studies have revealed that the aniline could be added as a reductant.[17] Herein, the nucleation process could be facilitated by the addition of aniline, and the increase of these nuclei densities significantly helps to reduce the size of the truncated octahedrons. If a truncated octahedron can be generated by cutting off six vertices from octahedron, where a was the distance from the vertex to the body center, then b was the height of each square pyramid, so the degree of truncation can be defined as b/a. In addition to the aniline concentration, the degree of truncation of the as-prepared nanocrystals depended on the molar ratio between benzoic acid and aniline. The reactions under the same conditions but lower molar ratio

dx.doi.org/10.1021/ja302606d | J. Am. Chem. Soc. 2012, 134, 8975–8981

yield products with a much greater degree of truncation. On the basis of the above results, the aniline was intentionally introduced as a coreductant and growth inhibition agent. Unlike the typical octahedral $PtNi_2$ alloy, the elemental map of the truncated octahedral $PtNi_2$ NPs showed that a greater quantity of Pt segregated at the edges of the particles and Ni appeared more centrally located (Figure 1g). This structure of uneven distribution was further verified by the following line scan of an individual particle (Figure S5 of the SI).

Cubic Pt_xNi_{1-x} ($0 < x < 1$) Nanocrystals. Previous studies have revealed that the carbon monoxide and bromide species could be selectively adsorbed onto Pt {100} crystal faces and induce the formation of nanocubes.[18,19] Here we successfully extended this method to the preparation of well-defined Pt−Ni alloy nanocubes of a broad range of compositions, notably without compromising the shape control. The as-prepared cubic particles have an average diagonal length of 16.1 ± 1.7 nm and surrounded by six equivalent {100} facets. To better understand the role of CO and KBr in the formation of our Pt−Ni nanocubes, we carried out control experiments (Figure S6 of the SI). Under otherwise identical conditions, the Pt−Ni nanocube obtained in absence of KBr had slightly changed from perfect nanocube to nanocube with rounded corners and the yield of nanocube decreased (from 95% to 60%). However, in the absence of CO, mixed morphologies (30% nanorods, 40% nanocubes, and 30% irregular shapes) were observed. These control experiments implied that the CO molecules were adsorbed more strongly onto the {100} faces than that of the bromide ion, although the addition of bromide ion could also improve the yield of nanocubes.

Ni Nanocrystals. This facile protocol could also be applied to the syntheses of Ni octahedrons with an average size of 40 ± 4.5 nm, albeit at an elevated temperature of 200 °C when benzaldehyde was used as an extra reductant (Figure 2a). Similarly, the truncated octahedral Ni with an average size of 25.2 ± 4.3 nm was synthesized when aniline replaced benzoic acid and benzaldehyde. Unfortunately, this route could not be extended to the synthesis of Ni nanocubes. This difference between the syntheses of Pt−Ni alloy and Ni in reaction temperatures could be understood by invoking a noble-metal-induced-reduction process.[20] While preformed Pt (0) species was believed to facilitate the reduction of Ni (II) to Ni (0) in the growth of Pt_xNi_{1-x} ($0 < x < 1$) nanocrystals, this process was not operative in the Ni synthesis. It is intriguing that these magnetic Ni octahedrons spontaneously assembled into large-scale one-dimensional nanostructures on copper grid after the ethanol was evaporated (Figure 2b−d). The observed aligning of Ni nanocrystals might be a result of their magnetic anisotropy as described by the Stoner−Wohlfarth model,[21] which found support in several studies on the relationship between the particles' self-assemble behavior and their magnetic property.[22−24] The HRTEM of as-synthesized Ni NPs showed lattice fringes of 0.204 nm, which could be assigned to {111} planes of Ni in face-centered cubic (fcc) phase (Figure 2e,f,i,j). Importantly, our method is found to be generally applicable to the synthesis of other water-soluble nanocrystals such as RhNi, PdNi, PdCu, and PtCu with excellent monodispersity and crystallization (Figure S9 and S10 of the SI).

The X-ray diffraction (XRD) patterns (Figure S8 of the SI) of all these nanocrystals could be indexed to {111}, {200}, and {220} diffractions with the peak positioned between those of Pt (JCPD-04−0802) and Ni (JCPD-04−0850) standard peak. We noted that the peaks continuously shifted from the Pt standard peaks to Ni standard ones when the content of Ni increases. The atomic ratios between Pt and Ni were further verified by Energy-dispersive X-ray spectroscopy (EDX) (Figure S4 of the SI) and ICP-AES (Table S5 of the SI). These data suggest that the composition of the product could be effectively controlled by choice of ratios between the two precursors.

It is important to note two features of our method: the use of phenyl organic molecules as growth inhibition agents and PVP as the capping agent. On the one hand, several groups have reported the shape control synthesis of Pt-based alloys, intermetallics and heterostructures,[25−27] which usually involved the use of metal carbonyls such as $W(CO)_6$[28] or CO.[29] In these methods, favorable growth of Pt nanocube was mainly credited to the strong binding of CO[30] or bromide anion[31] to Pt. In contrast, in our method benzoic acid and aniline played a crucial role in the growth of Pt−Ni octahedron and truncated octahedron (see control experiments in Figures S3 and S4 of the SI), probably due to their adsorption effect that suppresses crystal growth in certain direction. The adsorption effect of phenyl organic molecules were well documented, such as on metal (Au,[32] Pt,[33] Ni,[34] etc.), on oxides[35] and on carbon materials.[36] This controlling effect of the phenyl organic molecules was substantiated by the fact that substituting benzoic acid with salicylic acid or sodium benzoate also resulted in the formation of octahedrons (Figure S3d,e of the SI).

On the other hand, the commonly used solvents such as oleylamine, oleic acid, and octadecene in NP syntheses usually resulted in catalysts of low activity and selectivity, possibly due to the presence of long-chain capping agents and strong chemical bonds on the NP's surface.[37] Postsynthetic washing of the alkyl ligands and loading on to a solid support such as activated carbon were necessary to achieve desired performance. However, our Pt−Ni nanocrystals prepared in the presence of PVP could be dispersed in several polar solvents (Figure 3a) and used without any post treatment (vide infra).

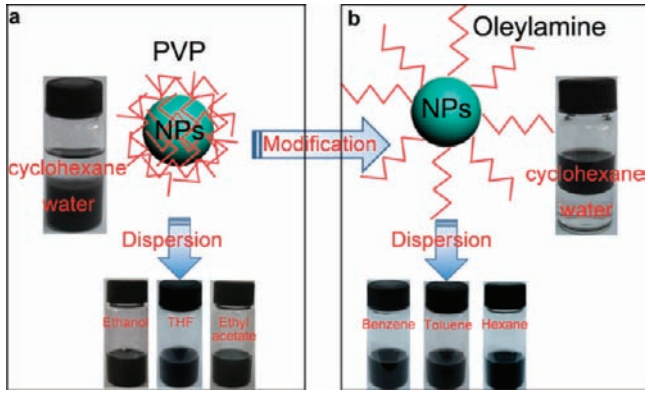

Figure 3. (a) The dispersions of PVP-capped $PtNi_2$ NPs in different polar solvents. (b) The dispersions of oleylamine-capped $PtNi_2$ NPs in different nonpolar solvents after surface modification.

Catalytic Performance in the Hydrogenation Reactions. Next, we tested our nanocrystals in catalytic reactions in order to probe their structure−activity relationship, which would shed light on further application studies. To this end, we chose hydrogenation of benzalacetone, styrene, and nitrobenzene as the laboratory test reactions (Figure 4), where heterogeneous catalysts have attracted great attention for their ease of their separation and recycling and benchmark reactivity is known. Notably, bimetallic catalysts are intriguing for

dx.doi.org/10.1021/ja302606d | J. Am. Chem. Soc. 2012, 134, 8975−8981

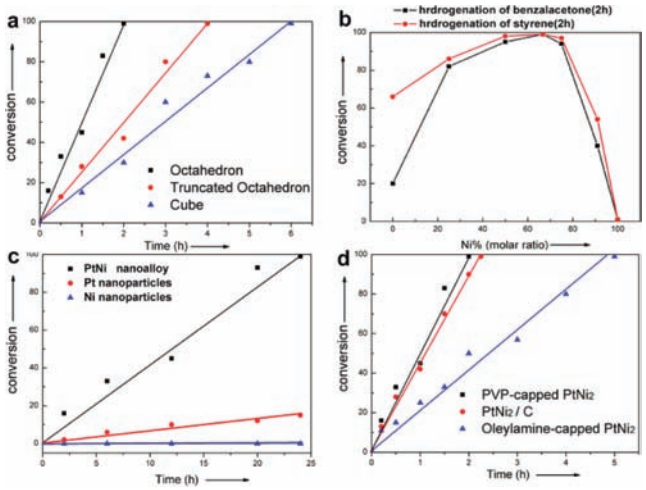

Figure 4. (a) Conversion % as a function of time in hydrogenation of benzalacetone with $PtNi_2$ octahedral, truncated octahedral and cubic nanocrystals. (b) Conversion % in a 2 h time of hydrogenation reactions of benzalacetone and styrene at rt under 1 atm H_2 pressure with octahedral NPs of different compositions. (c) Conversion % as a function of time in hydrogenation of nitrobenzene with $PtNi_2$, Ni, and Pt octahedrons. (d) Conversion % as a function of time in hydrogenation of benzalacetone with PVP-capped $PtNi_2$, "cleaned" $PtNi_2$/C (10% loading) and oleylamine-capped $PtNi_2$ octahedrons.

possible synergistic effects[38] that allow the hydrogenation reactions under relatively mild conditions. These features make the hydrogenation reactions suitable models for our preliminary tests.

Scheme 1. Hydrogenation of Benzalacetone, Styrene, and Nitrobenzene

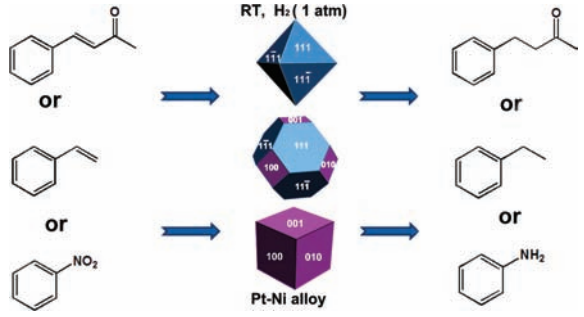

We first studied the shape-activity dependence (Figure 4a) in THF after screening results showed that THF, ethanol and ethyl acetate were equally capable solvents (Table S2 of the SI). To this end, three types of nanocrystals [i.e., Ni, Pt, and Pt_xNi_{1-x} $(0 < x < 1)$] with comparable size (Pt and Pt–Ni alloy: 12 ± 1 nm, Ni: 40 nm) and different shapes (octahedron, truncated octahedron, and cube) were tested to ensure a meaningful comparison. It is interesting to note that the catalyst activity in hydrogenation of benzalacetone increases with the increased percentage of {111} facets,[39] corresponding to the shape evolution from cube through truncated octahedron to octahedron. Next, we examined the composition-activity dependence using octahedral nanocrystals of different Pt/Ni ratios (Figure 4b). Overall, bimetallic nanoalloy catalysts are more active than their monometallic counterparts, in the order of $PtNi_2$ > PtNi ≈ $PtNi_3$ > Pt_3Ni > $PtNi_{10}$ > Pt > Ni, considering both the thermodynamic and kinetic factors. The same trend was also observed in the hydrogenation of styrene with these Pt–Ni octahedrons (Table S3 of the SI). The Turnover frequencies (TOF) per surface atoms of the four types of catalysts were further calculated (Table 1). The

Table 1. Turnover Frequencies [TOFs (h^{-1})] of the Hydrogenation of Benzalacetone Catalyzed by Various Catalysts[a]

entry	catalyst	average size (nm)	composition[b]	TOFs (h^{-1})
1	Pt octahedron	11.9		23
2	$PtNi_2$ octahedron	11.8	0.37:0.63	139
3	Ni octahedron[c]	40.0		
4	$PtNi_2$ truncated octahedron	12.5	0.36:0.64	114
5	$PtNi_2$ cube	11.2	0.35:0.65	95

[a]Conditions: substrate (0.5 mmol), 2 mol % catalyst with respect to the substrate and THF solvent (2.5 mL) were stirred under hydrogenation balloon/room temperature conditions. [b]The compositions were measured by ICP-AES. [c]Considering the ratio between surface area and volume, the amounts of Ni was 4 mol % respect to the substrate.

calculation method is detailed in the SI. The TOF measured using octahedral $PtNi_2$ was up to 6-times higher than that measured using octahedral Pt catalyst. The obtained TOFs for octahedral, truncated octahedral, and cubic $PtNi_2$ were 139, 114, and 95 h^{-1}, respectively. The higher catalytic performance can be ascribed to the high percentage of {111} facet. It was very satisfying to see that our best catalyst $PtNi_2$ octahedrons achieved 100% conversion with nearly 100% selectivity in 2 h at room temperature under atmospheric H_2 pressure. $PtNi_2$ octahedrons could effect both hydrogenation reactions 0 °C albeit at a slightly decreased rate (Table S2 of the SI), which is difficult with previously reported catalysts.

We then evaluated $PtNi_2$ octahedron in the hydrogenation reactions of nitrobenzene (Figure 4c), a more challenging reaction and important industrial process. It was again to our delight that nitrobenzene was quantitatively converted to aniline in 24 h (Table S4 of the SI). Consistent with the previous observation, $PtNi_2$ nanocrystals are substantially more active than the monometallic Pt and Ni nanocrystals, while the Ni nanocrystals show no activity at all. The oxidation state of octahedral $PtNi_2$ and octahedral Ni nanocrystals were measured by X-ray photoelectron spectroscopy (XPS). The surface information about $PtNi_2$ alloy revealed the Pt 4f7/2 and 4f5/2 had a binding energy of 71.3 ev and 74.6 ev, characteristic of Pt (0). The Ni 2p1/2 and 2p3/2 were 869.9 ev and 852.8 ev, respectively, which corresponded to the Ni (0). There was no oxidized Pt or Ni detected in the $PtNi_2$ alloy sample. In contrast, the XPS results showed that the surfaces of octahedral Ni nanocrystals were dominated by a thin layer of oxidized Ni.[40] We speculate that the fresh-prepared Ni was gradually oxidized by the oxygen in air to form this stable phase. In addition, previous study has revealed that the low activity of octahedral Ni catalyst could be contributed to the inertness of this thin layer of Ni (II).[41] These data collectively suggest that shape and composition indeed play an important role in dictating the catalysts' activity, suggesting possible enhanced activity on certain crystal facets and alloy surfaces.

One of the major goals in current heterogeneous catalyst research is to design nanocatalysts with good compatibility with complex reaction systems. Lastly, we examined the capping

dx.doi.org/10.1021/ja302606d | J. Am. Chem. Soc. 2012, 134, 8975–8981

agent-activity dependence (Figure 4d). We prepared the oleylamine-capped $PtNi_2$ nanocrystals through a ligand exchange process (Figure 2b) and a "cleaned" $PtNi_2/C$ (10% loading) catalyst (Figure S14 of the SI) (for details see SI). The oleylamine-capped nanocrystals are much less active toward hydrogenation of benzalacetone, while the PVP-capped nanocrystals show similar activity to that of the "cleaned" $PtNi_2/C$ catalyst, underlying the superiority of PVP as the capping agent that exempted the catalyst from postsynthesis treatment.[42] Ecologically friendly catalysts, especially those involving precious metals, underscore the emphasis of green chemistry. Unlike the organic syntheses that are routinely performed in nonaqueous solution, nature carries out enzymatic transformations on all organic molecules in water.[43] For their excellent compatibility with hydrophilic solvents without losing activity, the as-prepared water-soluble catalysts could find important applications in green chemistry and biology.[44]

Importantly, the catalysts could be recycled at least five times without observable decay of activity (Table S1 of the SI). TEM study of all spent catalysts found no obvious aggregation or shape change (Figure S15 of the SI), suggesting excellent stabilities of our nanocrystals under these reaction conditions. Upon completion of the reaction, the $PtNi_2$ catalyst could be easily separated by a magnet from the reaction mixture (Figure S13 of the SI) for the next cycle use.

CONCLUSIONS

In summary, we have developed a general method to synthesize water-soluble Pt, Pt_xNi_{1-x} ($0 < x < 1$), and Ni nanocrystals with uniformly controlled shapes and compositions. In our model hydrogenation reactions, the catalyst activity is positively related to the percentages of exposed {111} facets. Bimetallic nanoalloy catalysts are more active than their monometallic counterparts, suggesting a synergistic effect between the two metals. Using PVP as the capping agent exempted the catalyst from postsynthesis treatment without compromising the catalyst's solubility, activity, and recyclability. The general and facile synthesis of the nanocrystals, coupled with their high activity and stability, warrant further mechanistic and application studies of these nanocrystals. Research along these lines is currently ongoing in our laboratories and will be reported in due course.

ASSOCIATED CONTENT

Supporting Information

Pt, Pt_xNi_{1-x} ($0 < x < 1$), and Ni nanocrystals control experiments synthesis, characterization, and their catalytic hydrogenation reactions. This material is available free of charge via the Internet at http://pubs.acs.org.

AUTHOR INFORMATION

Corresponding Author

whe@tsinghua.edu.cn, ydli@mail.tsinghua.edu.cn

Notes

The authors declare no competing financial interest.

ACKNOWLEDGMENTS

This work was supported by the State Key Project of Fundamental Research for Nanoscience and Nanotechnology (2011CB932401 and 2011CBA00500), the National Natural Science Foundation of China (Grant Nos. 20921001 and 21131004). W.H. gratefully acknowledges the Tsinghua-Peking Center for Life Sciences for generous financial support.

REFERENCES

(1) Habas, S. E.; Lee, H.; Radmilovic, V.; Somorjai, G. A.; Yang, P. *Nat. Mater.* **2007**, *6*, 692−697.
(2) Huang, X. Q.; Tang, S. H.; Zhang, H. H.; Zhou, Z. Y.; Zheng, N. F. *J. Am. Chem. Soc.* **2009**, *131*, 13916−13917.
(3) Niu, Z. Q.; Peng, Q.; Gong, M.; Rong, H. P.; Li, Y. D. *Angew. Chem., Int. Ed.* **2011**, *50*, 6315−6319.
(4) Newton, M. A. *Chem. Soc. Rev.* **2008**, *37*, 2644−2657.
(5) Bing, Y. H.; Liu, H. S.; Zhang, L.; Ghosh, D.; Zhang, J. *J. Chem. Soc. Rev.* **2010**, *39*, 2184−2202.
(6) Daniel, M. C.; Astruc, D. *Chem. Rev.* **2004**, *104*, 293−346.
(7) Stamenkovic, V. R.; Fowler, B.; Mun, B. S.; Wang, G. F.; Ross, P. N.; Lucas, C. A.; Markovic, N. M. *Science* **2007**, *315*, 493−497.
(8) Wu, J. B.; Zhang, J. L.; Peng, Z. M.; Yang, S. C.; Wagner, F. T.; Yang, H. *J. Am. Chem. Soc.* **2010**, *132*, 4984−4985.
(9) Cailuo, N.; Oduro, W.; Kong, A. T. S.; Clifton, L.; Yu, K. M. K.; Thiebaut, B.; Cookson, J.; Bishop, P.; Tsang, S. C. *ACS Nano* **2008**, *2*, 2547−2553.
(10) Wu, Y. E.; Wang, D. S.; Zhao, P.; Niu, Z. Q.; Peng, Q.; Li, Y. D. *Inorg. Chem.* **2011**, *50*, 2046−2048.
(11) Ueno, S.; Shimizu, R.; Kuwano, R. *Angew. Chem., Int. Ed.* **2009**, *48*, 4543−4545.
(12) Harris, P. J. F. *Nature* **1986**, *323*, 792−794.
(13) Xu, R.; Xie, T.; Zhao, Y.; Li, Y. *Nanotechnology* **2007**, *18*, 055602.
(14) Schatz, A.; Reiser, O.; Stark, W. J. *Chem.—Eur. J.* **2010**, *16*, 8950−8967.
(15) Serna, P.; Corma, A. *Science* **2006**, *313*, 332−334.
(16) Zhu, Y.; Qian, H. F.; Drake, B. A.; Jin, R. C. *Angew. Chem., Int. Ed.* **2010**, *49*, 1295−1298.
(17) Tan, Y.; Xue, X.; Peng, Q.; Zhao, H.; Wang, T.; Li, Y. *Nano Lett* **2007**, *7*, 3723−3728.
(18) Tsung, C.-K.; Kuhn, J. N.; Huang, W.; Aliaga, C.; Hung, L.-I.; Somorjai, G. A.; Yang, P. *J. Am. Chem. Soc.* **2009**, *131*, 5816−5822.
(19) Bratlie, K. M.; Lee, H.; Komvopoulos, K.; Yang, P.; Somorjai, G. A. *Nano Lett.* **2007**, *7*, 3097−3101.
(20) Wang, D. S.; Li, Y. D. *J. Am. Chem. Soc.* **2010**, *132*, 6280−6281.
(21) Stoner, E. C.; Wohlfarth, E. P.; Ieee, T. *Magn.* **1991**, *27*, 3475−3518.
(22) Ku, J. Y.; Aruguete, D. M.; Alivisatos, A. P.; Geissler, P. L. *J. Am. Chem. Soc.* **2011**, *133*, 838−848.
(23) Alphandéry, E.; Ding, Y.; Ngo, A. T.; Wang, Z. L.; Wu, L. F.; Pileni, M. P. *ACS Nano* **2009**, *3*, 1539−1547.
(24) Petit, C.; Russier, V.; Pileni, M. P. *J. Phys. Chem. B* **2003**, *107*, 10333−10336.
(25) Ahrenstorf, K.; Albrecht, O.; Heller, H.; Kornowski, A.; Gorlitz, D.; Weller, H. *Small* **2007**, *3*, 271−274.
(26) Hou, Y. L.; Wang, C.; Kim, J. M.; Sun, S. H. *Angew. Chem., Int. Ed.* **2007**, *46*, 6333−6335.
(27) Zhang, J.; Fang, J. Y. *J. Am. Chem. Soc.* **2009**, *131*, 18543−18547.
(28) Zhang, J.; Yang, H. Z.; Fang, J. Y.; Zou, S. Z. *Nano Lett.* **2010**, *10*, 638−644.
(29) Wu, J. B.; Gross, A.; Yang, H. *Nano Lett.* **2011**, *11*, 798−802.
(30) Wu, B. H.; Zheng, N. F.; Fu, G. *Chem. Commun.* **2011**, *47*, 1039−1041.
(31) Yin, A.-X.; Min, X.-Q.; Zhu, W.; Liu, W.-C.; Zhang, Y.-W.; Yan, C.-H. *Chem.−A Eur. J.* **2012**, *18*, 777−782.
(32) Katoh, K.; Schmid, G. M. B. *Chem. Soc. Jpn.* **1971**, *44*, 2007−2009.
(33) Horanyi, G.; Solt, J.; Nagy, F. *Acta Chim. Hung.* **1971**, *67*, 425−426.
(34) Neuber, M.; Zharnikov, M.; Walz, J.; Grunze, M. *Surf. Rev. Lett.* **1999**, *6*, 53−75.
(35) Pang, X.-Y.; Lin, R.-N. *Asian J. Chem.* **2010**, *22*, 4469−4476.
(36) Koh, M.; Nakajima, T. *Carbon* **2000**, *38*, 1947−1954.

(37) Mazumder, V.; Sun, S. H. *J. Am. Chem. Soc.* **2009**, *131*, 4588–4589.
(38) Nakamula, I.; Yamanoi, Y.; Imaoka, T.; Nishihara, H.; Yamamoto, K. *Angew. Chem., Int. Ed.* **2011**, *50*, 5830–5833.
(39) Mostafa, S.; Behafarid, F.; Croy, J. R.; Ono, L. K.; Li, L.; Yang, J. C.; Frenkel, A. I.; Cuenya, B. R. *J. Am. Chem. Soc.* **2010**, *132*, 15714–15719.
(40) LaGrow, A. P.; Ingham, B.; Cheong, S.; Williams, G. V. M; Dotzler, C.; Toney, M. F.; Jefferson, D. A.; Corbos, E. C.; Bishop, P. T.; Cookson, J. *J. Am. Chem. Soc.* **2012**, 855–858.
(41) Park, J.; Kang, E.; Son, S. U.; Park, H. M.; Lee, M. K.; Kim, J.; Kim, K. W.; Noh, H. J.; Park, J. H.; Bae, C. J.; Park, J. G.; Hyeon, T. *Adv. Mater.* **2005**, *17*, 429–434.
(42) Tsunoyama, H.; Ichikuni, N.; Sakurai, H.; Tsukuda, T. *J. Am. Chem. Soc.* **2009**, *131*, 7086–7093.
(43) Magdesieva, T. V.; Nikitin, O. M.; Levitsky, O. A.; Zinovyeva, V. A.; Bezverkhyy, I.; Zolotukhina, E. V.; Vorotyntsev, M. A. *J. Mol. Catal A: Chem.* **2012**, *353–354*, 50–57.
(44) Xia, Y. N.; Li, W. Y.; Cobley, C. M.; Chen, J. Y.; Xia, X. H.; Zhang, Q.; Yang, M. X.; Cho, E. C.; Brown, P. K. *Acc. Chem. Res.* **2011**, *44*, 914–924.